SENSITIVITY STUDY OF INPUT PARAMETERS IN MODELING FLAME SPREAD IN BENCH-SCALE EXPERIMENTS USING THE SPYRO MODEL IN FDS

Anna Troff, Manuel Osburg, Brandschutz Consult Ingenieurgesellschaft mbH Leipzig, Germany

Alexander Belt, Lukas Arnold, Forschungszentrum Jülich GmbH, Germany

Jonathan Hodges, Jensen Hughes, USA

1 INTRODUCTION

The heat release rate (HRR) of a burning solid material depends on the interaction of several physical phenomena, such as the decomposition of the condensed phase, the exothermic combustion reaction in the gas phase, and the transfer of heat back to the material surface. While the fire safety community has made significant progress in quantifying material and reaction properties in recent years,[1,2] it is still the focus of on going research in the community.[3] As a result, simplified engineering approaches are often used in performance-based design (PBD) in fire safety applications.

The scaling-based pyrolysis (SPyro) model is a recently developed engineering model to bridge the gap between detailed pyrolysis models and engineering practice. SPyro uses the concept of heat of gasification to scale a measured bench-scale material response to dynamic exposure conditions predicted within a computational fluid dynamics (CFD) model.[4] The model estimates the flame heat flux occurring in a cone calorimeter experiment to calculate the reference heat flux for use in scaling. To date, this heat flux has been estimated based on an empirical formulation for a cone calorimeter in a horizontal configuration. However, these results are often applied to predict material behavior in a vertical configuration, for example wall linings.

In this study, cone calorimeter experiments were conducted using cast black polymethyl methacrylate (PMMA) across a range of configurations, including both horizontal and vertical orientations. The experimental data were used to calibrate and validate the SPyro model, enabling cross-prediction between configurations. Furthermore, the SPyro model was also applied to simulate fire growth in another bench-scale experiment.

2 METHODOLOGY

In this paper, experimental results for cast black PMMA at two different scales were analyzed and used to simulate flame spread with SPyro. Cone calorimeter experiments[5] were performed to derive material parameters and to evaluate the accuracy of SPyro's HRR predictions at the bench-scale. Furthermore, lateral flame spread experiments in vertical orientation, conducted using the ISO 5658-2 apparatus,[6] served to assess the precision of flame spread simulations.

2.1 Material

The experiments and simulations in this study were conducted using cast black PMMA. For the cone calorimeter tests, PMMA from the same manufacturer (PMMA A) was used. In the lateral flame spread

experiments, a cast black PMMA from a different manufacturer (PMMA B) was employed. Additionally, one reference experiment using PMMA A was also conducted for comparison.

2.2 Experiments

The cone calorimeter experiments presented in this paper involved tests on cast black PMMA subjected to three external heat fluxes (25, 50, and 75 kW/m²), two material thicknesses (6 and 10 mm), and both horizontal and vertical orientations, see Figure 1a. Each configuration was tested in triplicate. To fill the retainer frame, ceramic fiber boards *Fire-Board 1260 (R.A. Schmidt – Feuerfest GmbH)* of varying thicknesses were used as backing material.

The bench-scale experiments were conducted following the setup and procedures outlined in ISO 5658-2[6], commonly referred to as the "lateral flame spread" (LFS) or "spread of flame" test, see Figure 2. In this test method, specimens are exposed to a well-defined field of radiant heat flux. The heat flux distribution was calibrated in accordance with ISO 5658-2 specifications. The specimen is mounted in a vertical orientation opposite a gas-fired radiant panel, which is angled at 15° relative to the specimen. This configuration creates a varying distance between the panel and the specimen along its height, resulting in a gradient of incident heat flux. During the test, the time to ignition, the extent of lateral flame spread (Figure 1b), and the time to flame extinguishment are recorded as functions of time. Calcium silicate boards (*PROMATECT®-LS*, 30 mm thick) were used as the backing material for these experiments.

Replicate testing at both scales show little variability from test to test. The single test A single test is considered adequate for the material PMMA A, which was used as the basis for the further investigations.
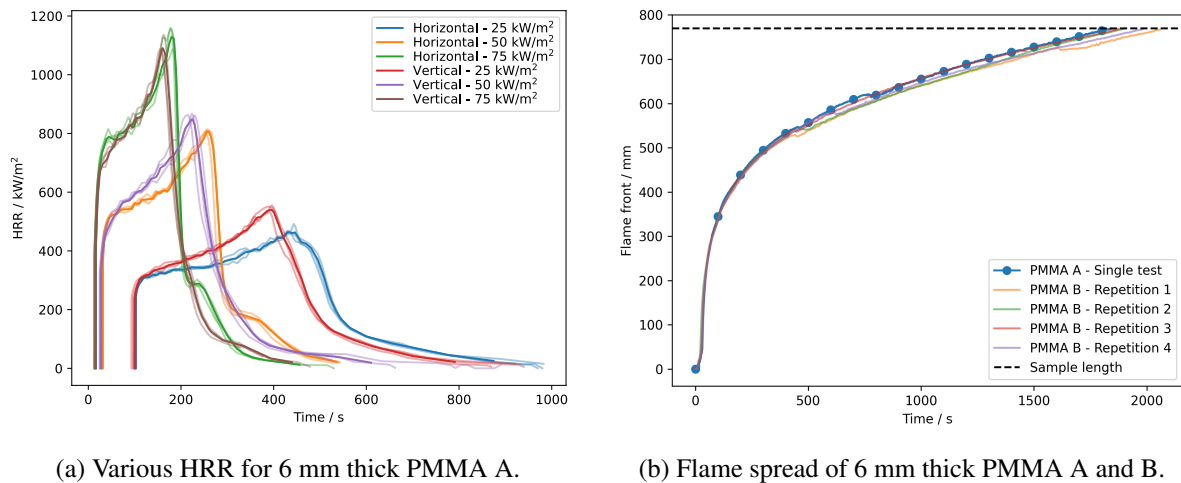

(a) Various HRR for 6 mm thick PMMA A. (b) Flame spread of 6 mm thick PMMA A and B.

Figure 1. Experimental data from (a) cone calorimeter and (b) flame spread experiments.

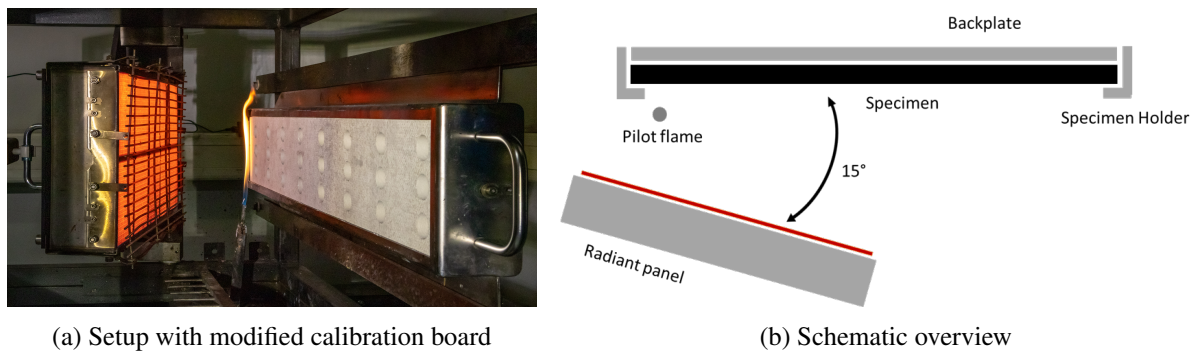(a) Setup with modified calibration board (b) Schematic overview

Figure 2. Representation of the lateral flame spread test setup in ISO 5658-2.

2.3 Modeling

This section describes the conditions, settings, and material parameters chosen for modeling the experiments with the Fire Dynamics Simulator (FDS). If not mentioned otherwise, FDS-6.9.1-0-g889da6a-release was used for the simulations.

2.3.1 Material parameters for PMMA and backing material

In addition to the HRR measured in the cone calorimeter for different irradiance levels, material thicknesses, and orientations, further parameters are required to simulate fire spread. The thermophysical and optical properties of cast black PMMA are taken from Fiola et al.[7] Simplified simulations of cone calorimeter tests with a cell size of 20 mm and an imprinted external heat flux were used to determine the ignition temperature and the heat of vaporization. For this, the generalized inverse modeling framework PROPTI[8] was used. The SCE-UA optimization algorithm[9,10,11] was used to find the values that were in the best agreement with the target data sets of the HRR curve, the ignition time, and the surface temperature during flaming combustion. Mean surface temperatures to be expected when testing PMMA under different heat exposures in the cone calorimeter were used from Rhodes and Quintiere.[12]

Table 1 contains a summary of the aforementioned material parameters. These parameters should be understood as effective parameters that should reflect the desired behavior of the model. Thicknesses and densities were measured. The thermophysical properties of the backing materials were taken from the respective product data sheets or estimated.

The parameters documented in Table 2 for characterizing the fuel chemistry of MMA and its combustion reaction are taken from different versions of the FDS Validation Guide.

1. Summary of (effective) material parameters.

Parameter	Unit	Cast Black PMMA	Backing Material (in ISO 5660-1)	Backing Material (in ISO 5658-2)
Thickness, d	mm	6 10	42 40	30
Density, ρ	kg/m^3	1,139	340	450
Conductivity, k	$W/(mK)$	0.16 (20 °C) 0.16 (122 °C) 0.015 (500 °C)	0.046 (0 °C) 0.061 (200 °C) 0.082 (400 °C)	0.08 (20 °C) 0.10 (200 °C) 0.11 (400 °C)
Heat Capacity, c_p	$kJ/(kgK)$	1.05 (20 °C) 1.90 (122 °C) 3.22 (500 °C)	1.1	0.95
Emissivity, ε	–	0.96	0.9	0.9
Absorption Coefficient, κ	m^{-1}	2,870	–	–
Ignition Temperature, T_{ign}	°C	341	–	–
Heat of Vaporization, h_v	kJ/kg	2,029	–	–

2.3.2 Cone Calorimeter

Two different approaches were used to model the cone calorimeter experiments. Vertical and horizontal geometries were considered in both approaches. Input data from horizontal cone calorimeter experiments were used as input in the horizontal geometry models to estimate the corresponding HRR curve. In contrast, the vertical geometry simulations used input data from both vertical and horizontal tests

2. Fuel chemistry and combustion reaction of MMA.

Property	Unit	Cone Calorimeter (ISO 5660-1)	Lateral Flame Spread (ISO 5658-2)
Formula	–	$C_5H_8O_2$	$C_5H_8O_2$
Heat of Combustion	MJ/kg	25.61	28.82
Specific Heat	$kJ/(kgK)$	1.48 (114 °C)	1.1
		1.90 (300 °C)	
CO Yield	kg/kg	0.010	0.010
Soot Yield	kg/kg	0.022	0.022
Radiative Fraction	–	0.33	0.31
Literature source		[13]	[14]

in two different cases. The optimized material parameters for black casted PMMA were used in both approaches.
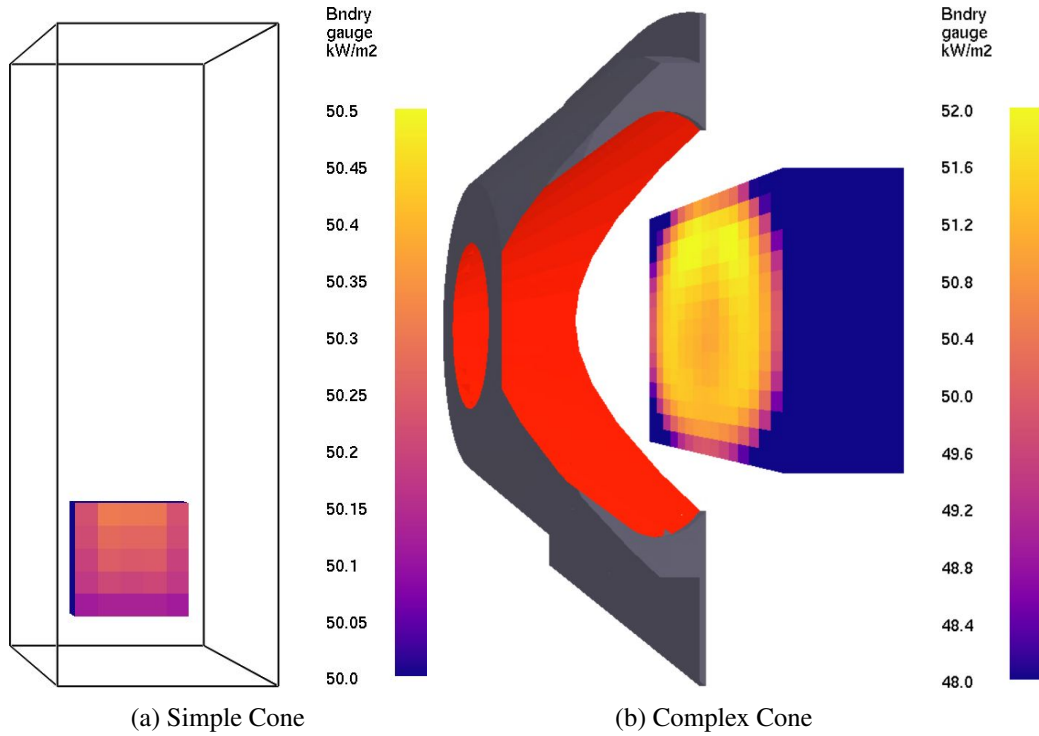

(a) Simple Cone   (b) Complex Cone

Figure 3. Cone calorimeter geometries with representation of the gauge heat flux at an irradiance of 50 kW/m² in vertical orientation before ignition.

The first configuration applies a uniform external flux directly to the surface. The computational domain has dimensions of 180 mm × 180 mm × 540 mm and a grid size of 20 mm. The sample surface is thus represented by 5 × 5 grid cells. This configuration is referenced herein as "Simple Cone" with uniform heat flux.

The second configuration uses a cone calorimeter geometry created by Hehnen[2] to better reproduce the variation of external flux on the sample surface. A grid size of 6.67 mm was chosen so that the sample could be resolved with 15 cells in each direction. An optimization procedure was used to determine the heater temperatures at an assumed emissivity of $\varepsilon = 0.9$. The heater temperatures were varied in the optimization simulations to achieve heat fluxes of 25, 50, and 75 kW/m² to a heat flux sensor (with default properties $T_{gauge} = 20\,°C$ and $\varepsilon_{gauge} = 1$) positioned 25 mm away and centered (see Figure 4a), both for

horizontal and vertical orientations. The radiation angles were varied from 100-500 and the results with 300 radiation angles were converged in both the horizontal and vertical orientations. The temperatures determined through optimization were the same in both the horizontal and vertical orientations with 634, 804, and 918 °C for the 25, 50, and 75 kW/m^2 exposures, respectively. Figure 4b compares the spatial variability of the gauge heat flux predicted by FDS on an isothermal sample surface at ambient with analytical solutions described by Wilson *et al.*[15] The white-dashed circle shows the analytical solution and the contours show the FDS model predictions. The heat fluxes on the vertical surface increase due to buoyancy and convection in the case of a non-isothermal material, as shown in Figure 4c. This geometry is referenced herein as a "Complex Cone" with distributed heat flux.

(a) Cone geometry, &GEOM^2 (b) Heat flux map on an inert sample   (c) Heat flux map on a CaSi-board
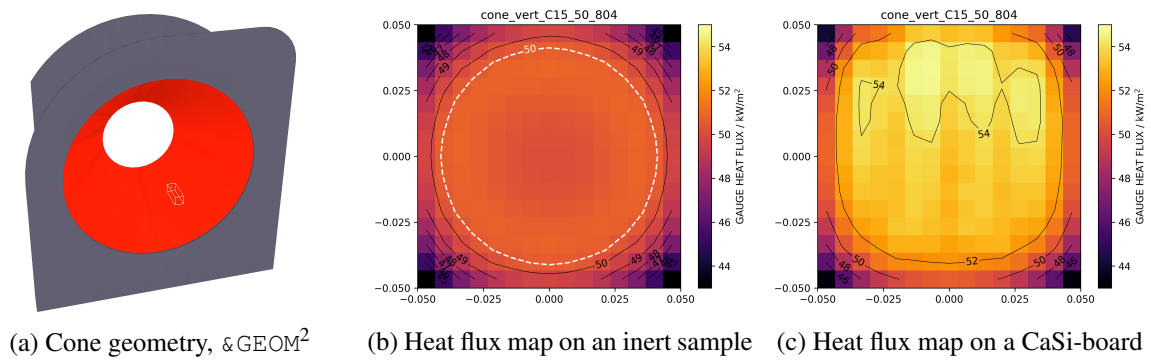
Figure 4. Representation of cone geometry and heat flux distribution in vertical orientation.

2.3.3 Lateral Flame Spread

A simplified representation of the lateral flame spread experiment was simulated in FDS. The computational domain, with dimensions of 960 mm × 80 mm × 180 mm was limited to the steel retainer frame and sample and its immediate surroundings (i.e., not including the 15° angled radiation panel). Simulations were carried out with grid sizes of 10 mm, 5 mm, 3.33 mm, 2.5 mm, 2 mm and 1.67 mm. LES was selected as the simulation mode. Otherwise, the default settings of FDS were left unchanged. The heat flux applied by the radiator was defined as an external flux on the sample surface at discrete intervals of 10 mm which the profile was derived from the calibration values for the incident heat flux given in ISO 5658-2.[6]
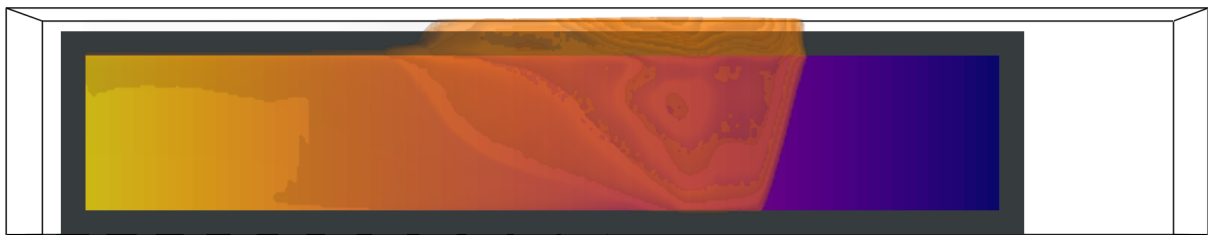

Figure 5. Simplified model for 2 mm fluid grid size at 600 s with visualization of flame propagation and the applied heat flux.

3 RESULTS AND DISCUSSION

3.1 Cone Calorimeter

Three pyrolysis configurations were modeled in both the "Simple Cone" and "Complex Cone" representations. The first case used data from horizontal cone calorimeter experiments with the SPyro model in the horizontal configuration (h-h). The second case was similar but used data from vertical cone

calorimeter experiments to predict burning in the vertical configuration (v-v). The third case uses data from horizontal cone experiments to predict the burning behavior in a vertical configuration (v-h).

Figure 6 shows the predictions for a 6 mm sample thickness with all three configurations using the "Simple Cone" representation. In all cases only the cone calorimeter experiment at 50 kW/m^2 and 6 mm thickness was used to estimate the HRR curve using SPyro. Table 3 provides the root mean square error (RMSE) between the simulation predictions and the experimental data for each case.

In all studied cases the time to ignition matched well between simulation and experiment. With one provided curve in this setup the HRR can be scaled to different heat fluxes and thicknesses, resulting in a similar error than recreating the reference curve (50 kW/m^2, 6 mm). However, it is important to note, that PMMA showed a consistent behavior with cone tests in different thicknesses and heat fluxes and is particularly well-posed to the SPyro method. The HRR dips before the peak in experimental data in horizontal orientation models. In addition, a systematic underestimation of the HRR can be seen in all curves in the vertical orientation. The predicted HRR was lower in the case where the horizontal cone data was used for scaling than with vertical data.
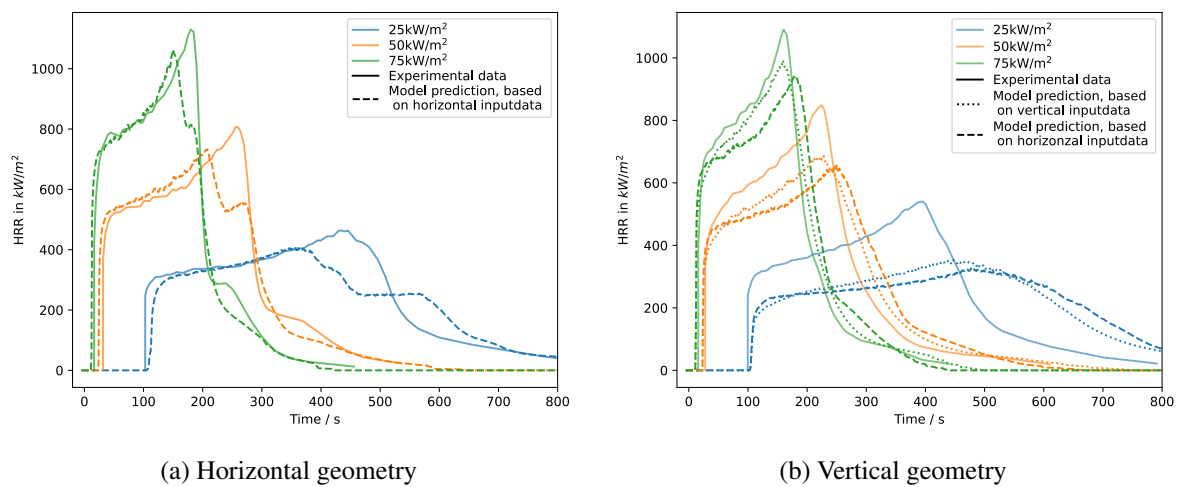

(a) Horizontal geometry   (b) Vertical geometry

Figure 6. Comparison of HRR estimations using SPyro in "Simple Cone" geometry with uniform imprinted heat flux at 6 mm sample thickness

3. Comparison experimental data and simulation using RMSE ("Simple Cone")

	6 mm 25 kW/m^2	6 mm 50 kW/m^2	6 mm 75 kW/m^2	10 mm 25 kW/m^2	10 mm 50 kW/m^2	10 mm 75 kW/m^2	Mean
			FDS version 6.9.1				
h-h	1.66	1.76	1.70	2.06	2.38	2.67	2.04
v-v	2.96	1.53	1.17	3.16	1.89	1.89	2.10
v-h	3.36	2.30	2.09	3.80	2.85	3.02	2.90

Figure 7 shows similar predictions with the "Complex Cone" geometry and a 6 mm sample thickness, and Table 4 provides the RMSE for the full set of simulations. Each of these simulations used all 5 curves of the conducted cone experiments (different heat fluxes and thicknesses) except the target curve to estimate the HRR curve using SPyro. The HRR is overestimated in the horizontal geometry, although to a lesser extent than in the "Simple Cone" vertical orientation. The difference is more significant at the lower incident heat flux. In contrast, the vertical orientation simulations with vertical input data align well with the experimental data. The predicted HRR is slightly lower in the vertical configuration when horizontal data is used as an input, which makes sense since the HRR was lower in the input data. The
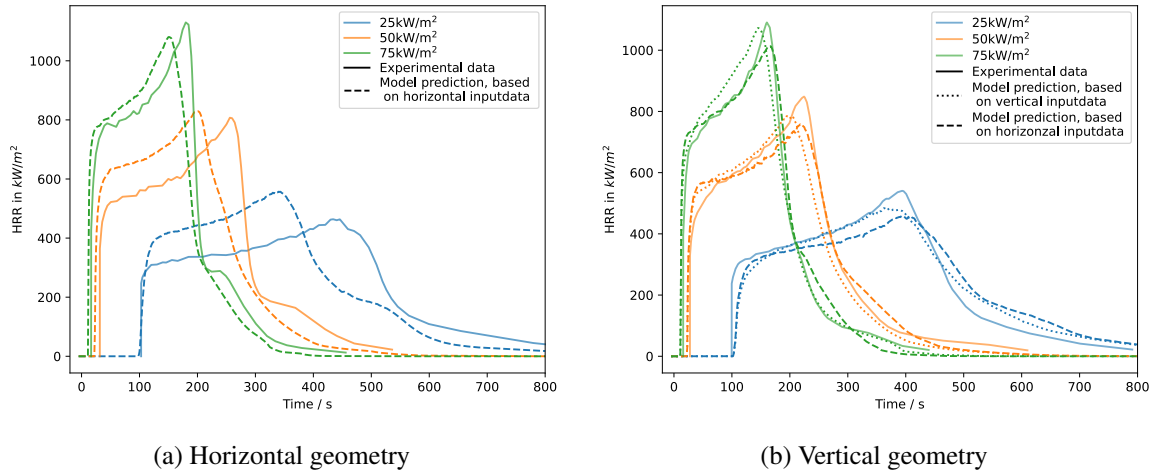
(a) Horizontal geometry

(b) Vertical geometry

Figure 7. Comparison of HRR estimations using SPyro in "Complex Cone" geometry with locally diverged heat flux at 6 mm sample thickness

results in the vertical orientation with the"Complex Cone" model matched the experimental data better than in the horizontal orientation. This represents an opposite tendency to the "Simple Cone" cases. This is in part due to the differences in heat flux on the sample surface; however, the different grid resolutions could also be a factor.

4. Comparison experimental data and simulation using RMSE ("Complex Cone")

	6 mm 25 kW/m^2	6 mm 50 kW/m^2	6 mm 75 kW/m^2	10 mm 25 kW/m^2	10 mm 50 kW/m^2	10 mm 75 kW/m^2	Mean
			FDS version 6.9.1				
h-h	2.50	2.80	2.23	4.03	3.76	2.64	2.99
v-v	0.97	1.27	1.31	1.72	1.67	1.60	1.42
v-h	1.25	1.00	1.28	1.37	1.52	2.58	1.50
			FDS version 6.10.1				
h-h	2.05	2.12	1.57	3.13	2.63	2.89	2.40
v-v	1.43	1.60	1.30	1.63	2.49	2.12	1.76
v-h	1.93	2.28	2.26	2.37	3.29	4.20	2.72

In addition, simulations with FDS version 6.10.1 were conducted to observe possible changes with updates to the SPyro submodel. In Table 4, the RMSE values for simulations with both FDS versions are shown. The parameter optimization for PMMA were revisited with FDS using 6.10.1. As an ignition temperature a value of 330 °C and for the heat of vaporization 1900 kJ/kg were optimized. The temperature values for the cone heater in the detailed cone calorimeter geometry were also revisited. The temperatures matched the values calculated for FDS 6.9.1.

The HRR curves in simulations with FDS 6.10.1 are lower than with 6.9.1 in all cases. Because of this, a better match can be seen in the horizontal test configuration. For the 75 kW/m^2 heat flux an underestimation of the HRR can be observed. In both cases of the vertical geometry a stronger underestimation of the HRR can be observed than in FDS 6.9.1.

3.2 Lateral Flame Spread

Figure 8 compares model predicted flame positions with different grid sizes with the experimentally determined flame positions. Figure 8a compares the fire spread prediction with data from different cone configurations: dotted lines based on vertical data and solid line based on horizontal data. Figure 8b compares fire spread with parameter optimization in solid lines with predictions using parameters taken from the literature[13] in the dotted lines which has a higher ignition temperature of 436 °C and no heat of vaporization. Both sets of simulations in Fig. 8b use data from the vertical cone configuration.
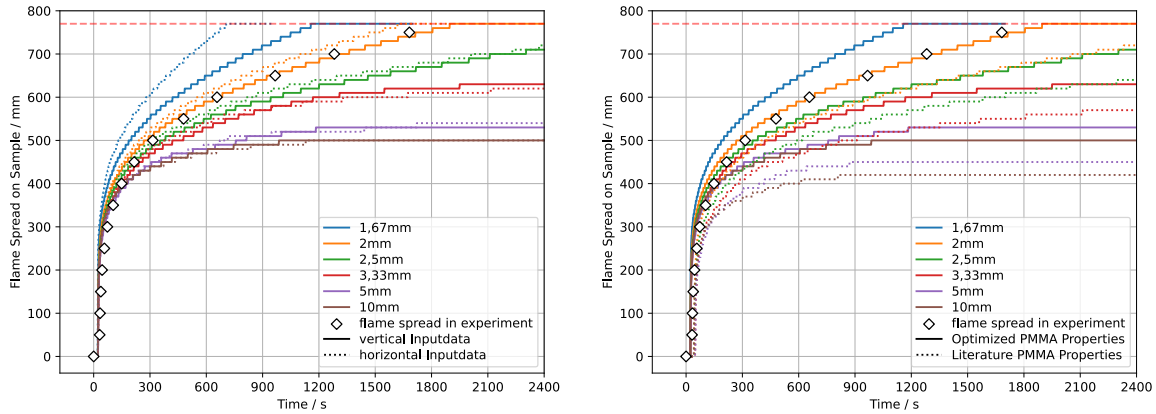
(a) Comparison vertical and horizontal orientation   (b) Comparison optimized and literature parameters[13]

Figure 8. Comparison of lateral flame spread in vertical orientation with black casted PMMA

In both orientations a strong grid size dependency can be seen in the predicted flame spread rates. The best agreement with the experiments is with a grid size of 2.0 mm for both vertical and horizontal input data. However, these results are not converged as the simulated flame spread is faster at the 1.67 mm resolution. The flame spread curves show a similar course when vertical and horizontal input datasets were used. This behavior is also described by Quaresma[16] for a similar setup that considers lateral flame spread over a horizontal sample. These simulations were conducted with FDS, using the complex pyrolysis modeling approach. The simulations also showed the closest agreement with experimental data at a grid size of 2 mm. An additional insight from Quaresma which was not explored in this study was variability observed based on the solid cell size.
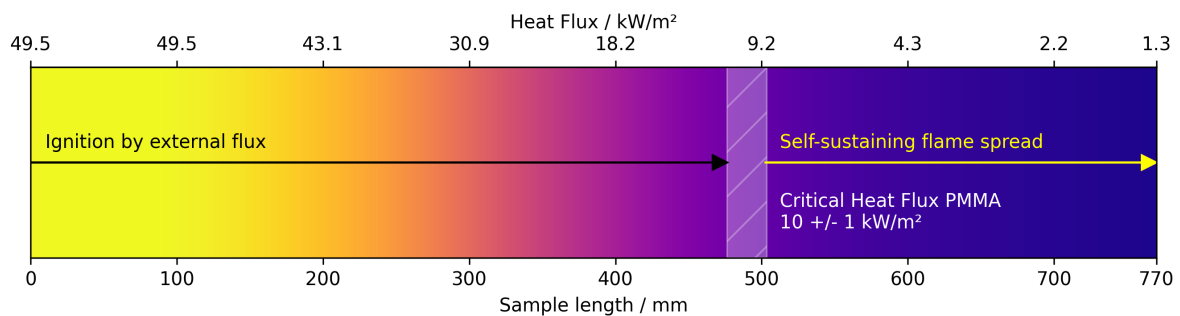

Figure 9. Representation of the critical heat flux of PMMA on sample in test setup ISO 5658-2.

Figure 8b shows the rate of flame spread is lower when the literature values for the ignition temperature and the default heat of vaporization are used compared with the optimized parameters. In addition, flame spread ends earlier at the coarser grid resolutions (e.g., at 420 mm compared to 500 mm with a 10 mm grid size).

These results can be explained in part by comparing the external radiative heat flux with the critical heat

flux of the sample, as shown in Fig. 9. Figure 9 compares the heat flux distribution on the sample surface in the test setup ISO 5658-2 as prescribed in the standard. The position on the sample surface is marked in which the critical heat flux of PMMA is reached. Until this marking, ignition can be achieved through the external flux by the heater element without an additional contribution from the burning sample. After this marking, self-sustained flame spread has to be considered.
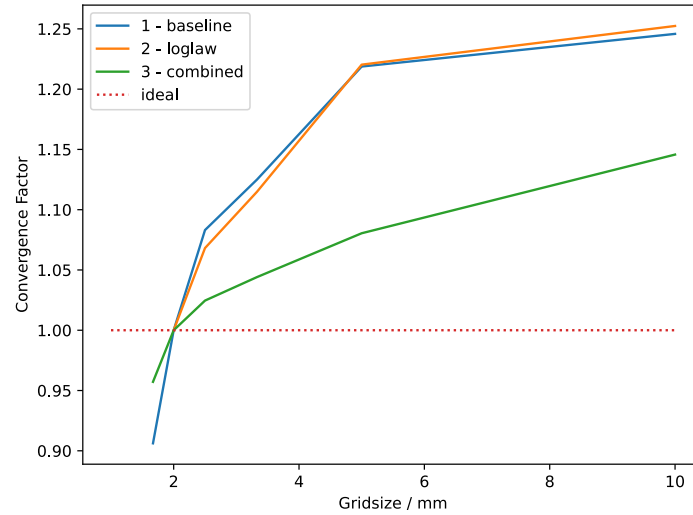

Figure 10. Difference between integrals of time dependent flame spread in experimental data and simulation.

One of the key findings from these simulations is that additional work is needed to reduce the impacts of grid resolution on predictions of flame spread rate. A convergence factor was defined in this work to evaluate the impact of different modeling parameters on the grid convergence. The grid convergence factor is defined as the difference in area under the curve in Fig. 8 between a target resolution and a fixed reference resolution normalized by the value at the fixed resolution (taken to be 2 mm in this case which aligned best with the experiments). Figure 10 compares the convergence factor in three configurations.

The first configuration shows the convergence in the baseline case described in this paper for reference which ranges from 0.91 at the finest resolution to 1.23 at the coarsest. The remaining cases adjusted parts of the simulation method related to convection, radiation, and extinction to evaluate these impacts. The second case changes from the default convection heat transfer model to use a log-law wall function for the temperature. This model had similar results to the base case. The third case introduces several changes. First, the limits on the radiation correction factor used to match a user-defined radiative fraction are extended to 0.1-1000. Second, a fixed heat transfer coefficient of 15 W/m^{2}K is used. And lastly, the gas phase flame extinction model is disabled which removes the link between the lower limit on oxygen concentration that can be reached and the local gas phase cell temperature. Under these changes, the convergence factor is closer to one than the base case, ranging from 0.96-1.12. While these changes do not completely explain the issues with grid convergence, they do point to areas in the software algorithm which impact grid convergence in flame spread in default conditions.

Additional insight can be obtained by evaluating the heat transfer to the surface, shown in Fig. 11. Figure 11 shows the gauge (at ambient reference temperature), convective (at heated surface temperature), and incident radiative heat flux and heat transfer coefficient along the sample at the time the flame front has reached the 500 mm position at each resolution (i.e., different simulation times, but similar position). A wide range of values are present in both the gauge heat flux and heat transfer coefficient across grid resolutions. The incident radiation at the leading edge in Fig. 11c is converged from 1.67 mm-3.33 mm. However, the convective heat flux shown in Fig. 11d is not converged at the leading edge. Comparing the 1.67 mm to the 3.33 mm resolution, the heat flux is almost 100 % higher. Based on these results, it is

hypothesized that the convective heat transfer calculation is the primary contributor to grid convergence issues seen in this model configuration.
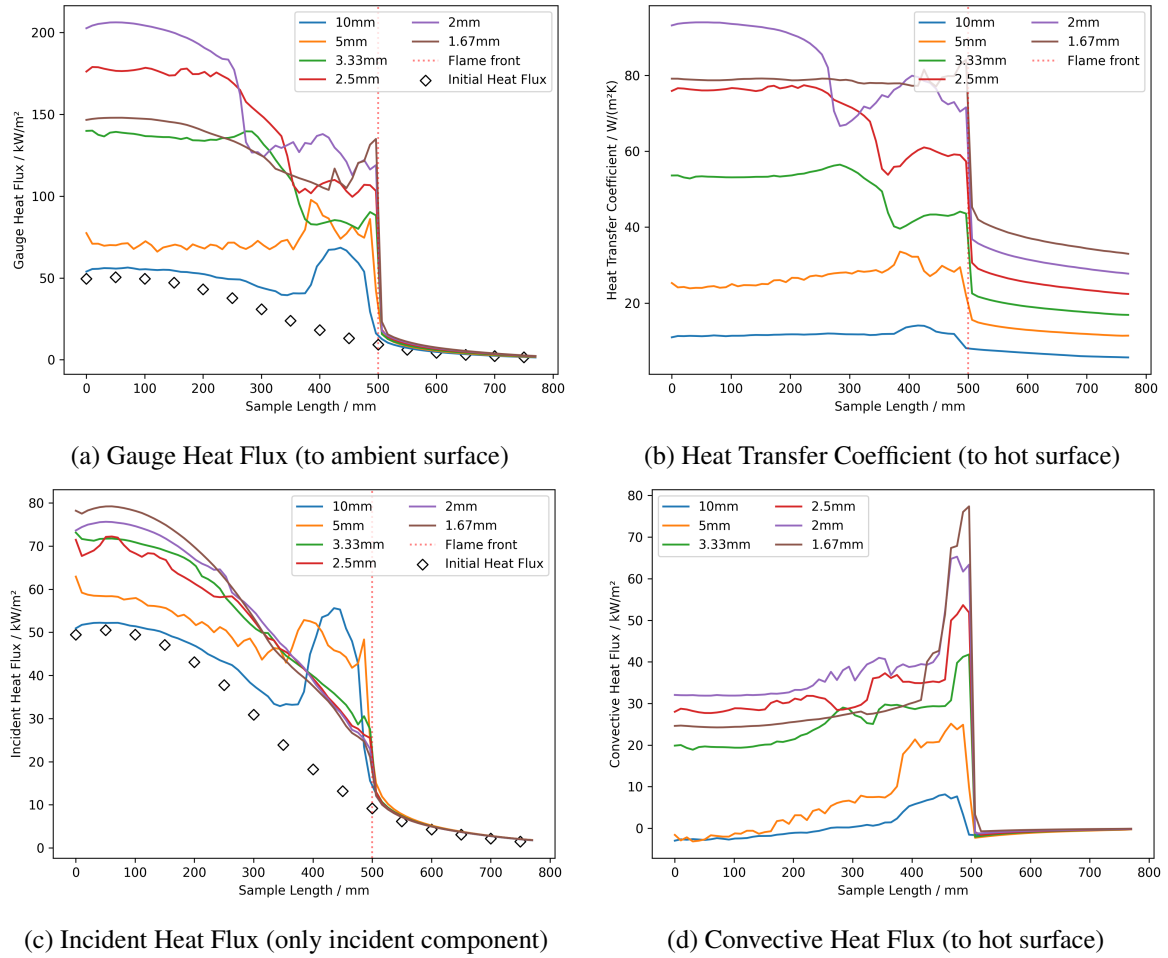

(a) Gauge Heat Flux (to ambient surface)

(b) Heat Transfer Coefficient (to hot surface)

(c) Incident Heat Flux (only incident component)

(d) Convective Heat Flux (to hot surface)

Figure 11. Centerline heat flux distribution along the sample for the baseline case.

4 CONCLUSION

The results from FDS simulations of two different bench-scale test setups were compared with experiments in this work. The test setups studied were cone calorimeter (ISO 5660-1) tests and lateral flame spread apparatus in a vertical orientation (ISO 5658-2). The SPyro model in FDS was used to predict the HRR and the rate of flame spread across the sample surface. Each configuration was simulated with multiple grid resolutions to evaluate the grid convergence of the results.

The cone calorimeter simulations used two different representations of the heat transfer from the cone, one with uniform heat flux and the other spatially varying. Both representations of the cone had different predictions in the horizontal and vertical orientations. The agreement in the horizontal orientation was closer when using the uniform heat flux, which is intuitive since a similar approach was used in the SPyro development. However, the agreement in the vertical orientation was better when using the spatially resolved cone heat fluxes. When horizontal input data was used for the vertical geometry, the estimated HRR using SPyro was lower than when vertical input data was used. This observation is consistent with the experimental data used. There are a few possible reasons for the difference observed in simulations with the two cone models is the different grid size or differences in the convective heat flux to the sample surface in the vertical and horizontal orientations. This different local heat flux is only accounted for in the detailed cone model. Another possible reason is the higher flame height between the sample surface

and the cone heater in the horizontal configuration. This could have a higher impact on the absorption of the radiation from the cone heater by the products of combustion and therefore on the incident heat flux to the sample surface.

The lateral flame spread in vertical orientation simulations demonstrated grid dependence across all tested cases. A grid resolution of 2 mm with effective parameters for IgnTemp and HOV provided good agreement with the experimental data. However, these results were not converged as a finer grid resolution resulted in a faster flame spread than observed in the experiments. The orientation of the cone calorimeter data used in the LFS simulations did not have a significant impact on the results at lower resolutions. However, the horizontal input data did result in a faster flame spread rate at the finest resolution of 1.67 mm. Flame spread to the end of the sample was predicted in the 1.67 mm and 2.0 mm resolutions. Flame spread stagnated beyond the section where the initiating heat flux dropped below the critical heat flux for PMMA at the coarser resolutions of 5-10 mm. Analysis of the heat fluxes along the sample surface showed a grid dependence of the convective heat flux along the leading edge whereas the incident radiative heat flux was converged. As a whole, these results point towards grid dependence with the convective heat transfer between the flame and sample surface. Future analysis investigating the sources of this grid dependence will improve the ability of designers to use CFD fire models to model fire growth.

ACKNOWLEDGMENTS

REFERENCES

[1] Stoliarov, S. I. and Y. Ding (2023). "Pyrolysis model parameterization and fire growth prediction: The state of the art". In: *Fire Safety Journal* 140, p. 103905. ISSN: 03797112. DOI: 10.1016/j.firesaf.2023.103905.

[2] Hehnen, T. and L. Arnold (Dec. 2023). "PMMA pyrolysis simulation – from micro- to real-scale". en. In: *Fire Safety Journal* 141, p. 103926. ISSN: 03797112. DOI: 10.1016/j.firesaf.2023.103926. (Visited on 11/13/2024).

[3] Babrauskas, V. (2016). "Heat Release Rates". In: *SFPE Handbook of Fire Protection Engineering, Fifth Edition*. Society of Fire Protection Engineers, pp. 799–904. ISBN: 9781493925650. DOI: 10.1007/978-1-4939-2565-0.

[4] Hodges, J. L. et al. (2023). "An engineering model for the pyrolysis of materials". In: *Fire Safety Journal* 141.September, p. 103980. ISSN: 0379-7112. DOI: 10.1016/j.firesaf.2023.103980.

[5] *ISO 5660-1:2015 - Reaction-to-fire tests - Heat release, smoke production and mass loss rate - Part 1: Heat release rate (cone calorimeter method) and smoke production rate (dynamic measurement)* (n.d.). ISO.

[6] *ISO 5658-2:2006 - Reaction to fire tests — Spread of flame - Part 2: Lateral spread on building and transport products in vertical configuration* (2006). ISO.

[7] Fiola, G. J., D. M. Chaudhari, and S. I. Stoliarov (Mar. 2021). "Comparison of Pyrolysis Properties of Extruded and Cast Poly(methyl methacrylate)". In: *Fire Safety Journal* 120, p. 103083. ISSN: 03797112. DOI: 10.1016/j.firesaf.2020.103083. URL: https://linkinghub.elsevier.com/retrieve/pii/S0379711219307301.

[8] Arnold, L. et al. (Jan. 2019). "Application cases of inverse modelling with the PROPTI framework". In: *Fire Safety Journal*. Num Pages: 15. ISSN: 03797112. DOI: 10.1016/j.firesaf.2019.102835.

[9] Duan, Q., S. Sorooshian, and V. Gupta (1992). "Effective and efficient global optimization for conceptual rainfall-runoff models". In: *Water Resources Research* 28.4, pp. 1015–1031. DOI: https://doi.org/10.1029/91WR02985. URL: https://agupubs.onlinelibrary.wiley.com/doi/abs/10.1029/91WR02985.

[10] Duan, Q., V. Gupta, and S. Sorooshian (1993). "Shuffled complex evolution approach for effective and efficient global minimization". In: *Journal of Optimization Theory and Applications* 76.3, pp. 501–521. DOI: https://doi.org/10.1007/BF00939380.

[11] Duan, Q., S. Sorooshian, and V. Gupta (1994). "Optimal use of the SCE-UA global optimization method for calibrating watershed models". In: *Journal of hydrology* 158.3-4, pp. 265–284.

[12] Rhodes, B. T. and J. G. Quintiere (Apr. 1996). "Burning rate and flame heat flux for PMMA in a cone calorimeter". In: *Fire Safety Journal* 26.3, pp. 221–240. ISSN: 03797112. DOI: 10.1016/S0379-7112(96)00025-2. URL: https://linkinghub.elsevier.com/retrieve/pii/S0379711296000252 (visited on 11/13/2024).

[13] McGrattan, K. (Apr. 2025). *Fire Dynamics Simulator, Technical Reference Guide, Volume 3: Validation*. Sixth Edition. 1018-3. NIST Special Publication. Revision: FDS-6.10.1-0-g12efa16. NIST.

[14] *fds/Validation/NIST_NRC_Parallel_Panels/FDS_Input_Files/PMMA_60_kW_1_cm.fds* (June 2023). URL: https://github.com/firemodels/fds/blob/84651732cd3e18a0f3034a9b5615bd296d5e8 Validation/NIST_NRC_Parallel_Panels/FDS_Input_Files/PMMA_60_kW_1_cm.fds.

[15] Wilson, M., B. Dlugogorski, and E. Kennedy (2003). "Uniformity Of Radiant Heat Fluxes In Cone Calorimeter". en. In: *Fire Safety Science* 7, pp. 815–826. ISSN: 18174299. DOI: 10.3801/IAFSS.FSS.7-815. (Visited on 03/04/2025).

[16] Quaresma, T. L. d. S. (2025). "Sensitivity Analysis on Flame Spread Simulation – Submitted". en. PhD thesis. Bergische Universität Wuppertal, Fakultät für Architektur und Bauingenieurwesen, Germany, p. 111.